

pubs.acs.org/acsapm Article

Dual-Cure Networks Designed for Property Modulation via High-Energy Radiation

Weiqing Xia, Samuel B. Hurvitz, Joshua Y. Lee, Scott E. Stapleton, and Daniel F. Schmidt*



Cite This: https://doi.org/10.1021/acsapm.3c00465



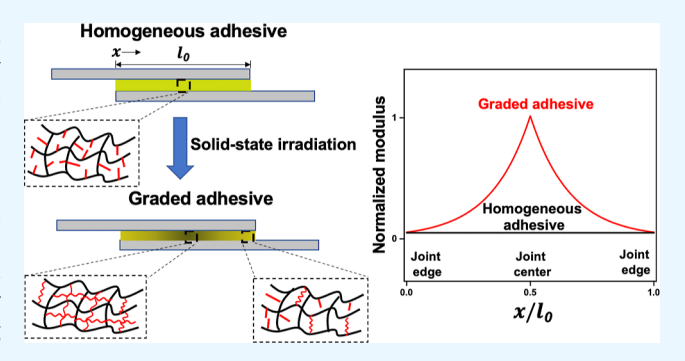
ACCESS

III Metrics & More

Article Recommendations

s Supporting Information

ABSTRACT: A functionally graded adhesive (FGA) is a specific class of functionally graded material whose properties can be locally modulated, enabling a more uniform stress distribution along a bonded joint. Motivated by the need to develop FGAs with well-defined and stable gradients in properties, a new approach is proposed involving the use of thermal/ionizing radiation dual-cure adhesives. To generate adhesives with dual-cure characteristics, a series of epoxy resin formulations containing a reactive liquid rubber-based additive that is rich in unsaturation have been developed. Networks are thermally cured and then subjected to γ irradiation, and their capacity to undergo secondary crosslinking reactions is examined via chemical, thermal, and mechanical



characterization. While the addition of large concentrations of liquid rubber additives can result in an initial reduction in properties such as modulus and glass transition temperature, their addition can significantly boost radiation sensitivity, enabling the realization of large, well-controlled variations in properties as a function of radiation dose. A facile method is then utilized to create materials with gradients in hardness, confirming the potential of such formulations to generate FGAs. Additionally, the behavior of these radiation sensitive resins is successfully described by a model proposed by Shibayama. This model provides a useful means to predict the glass transition temperatures of dual-cure epoxy resins following radiation-induced crosslinking and provides additional insights into molecular-level behavior of these networks. This effort highlights the promise of this generalized approach for the formation of FGAs based on the careful design and processing of systems sensitive to both thermal and radiation curing.

KEYWORDS: functionally graded adhesives, functionally graded materials, polymer networks, dual curing, high-energy radiation

■ INTRODUCTION

Functionally graded materials (FGMs) are advanced functional materials whose structure and/or properties are locally modulated in one or more dimensions. FGMs exhibit excellent performance in many fields of application and can surpass those of homogeneous materials. As a result, FGMs are not rare in nature. Bamboo is one example of a gradient structure that has been employed as a construction material for thousands of years. The graded structure can effectively reduce stress concentrations, producing a more uniform stress distribution. FGMs have also been designed to reduce residual stress levels caused by thermal expansion mismatch between substrates and coatings.

Polymer-based FGMs are of interest due to their applications in numerous high-technology fields ranging from aerospace to biology and electrical engineering. ^{4,5} A variety of formulations and methodologies to produce polymer-based FGMs have been investigated. ^{6–8} The success of FGMs leads to the thought of using such materials in adhesive joints. One major issue in conventional adhesive joints is the presence of stress concentrations at the overlap edge of the joints, where failure typically takes place. ⁹ One solution to generate more

uniform stress distributions within the joint is by designing a functionally graded structure along the bond line, thus producing what are referred to as functionally graded adhesives (FGAs).¹⁰ In general, the optimum structure of an FGA is usually a combination of rigid material at the center of the joint and ductile/soft material at the overlap edges to realize a more uniform stress distribution. FGAs have received attention since their potential to enhance joint strength was recognized conceptually, ^{11–13} but techniques to produce FGAs remain rare. ^{14,15} The specific "sandwich" structure of joints makes it inconvenient if not impossible to apply techniques used for generating FGMs in the context of FGA preparation. ¹⁶ For example, photocuring has been commonly used to prepare polymer-based FGMs, where a gradient in the properties of a UV-sensitive substrate can be modulated by local changes in

Received: March 7, 2023 Accepted: June 6, 2023



ACS Applied Polymer Materials

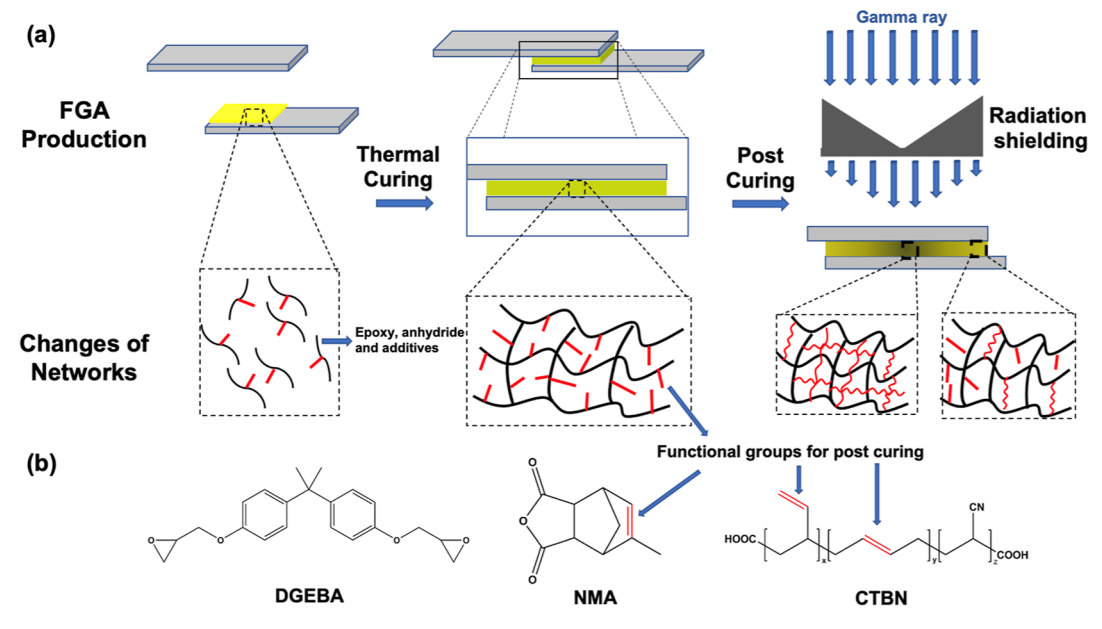


Figure 1. (a) Schematic illustration of the generalized approach proposed for the preparation of FGAs using dual-cure adhesives: conventional cure to stabilize the joint, followed by selective irradiation to induce further crosslinking in the solid state, thus generating the desired FGA structure and (b) epoxy, anhydride, and liquid rubber additives used in this work.

the transmittance of a photomask that is placed between the light source and the substrate during exposure. ¹⁷ However, the inability of light to penetrate typical adherend materials (e.g., metals and fiber-reinforced composites) has impeded the application of photocured systems in the context of FGA generation. ¹⁸

Approaches used to prepare FGAs can be divided into two basic categories: graded composition and graded cure along the joint. 14 The first approach involves either the manual application of adhesives with different properties or the inclusion of varying amounts of a second (soft or rigid) phase in the adhesive, resulting in local variations in composition and properties along the bond line. 19,20 This approach effectively produces stable gradients along the joint with a high degree of customization, but it is also a costly, labor-intensive method that is impractical for large-scale production, with relatively poor consistency and quality control. The second approach involves modulating the extent of cure of a single-component adhesive via localized external stimuli (typically heating) applied to the adhesive joint. Carbas et al. prepared FGAs by using localized heating along the bond line, where heating coils situated at the edges combined with cooling coils in the middle of a single lap joint resulted in gradient formation.²¹ Hu et al. recently reported a network with a broad gradient in hardness through local variations in postcuring temperature that may also enable the generation of FGAs.²² Such methods efficiently produce gradients in properties and have the potential to be automated, but one significant drawback is the potential instability of the gradient with time, especially when the joint is subjected to elevated temperatures. Because of this, the service temperature and long-term stability of FGAs fabricated by such methods may be limited.²³ As this discussion reveals, then, the primary challenge in the application of FGAs is still their manufacturing. Neither of the aforementioned approaches for FGA production provides a convenient, readily scalable means to generate a precisely controlled, consistent, and stable gradient in properties within an adhesive joint.

To fulfill this goal, the work described here involves the use of ionizing radiation as an effective means to fabricate FGAs. ^{16,24} Figure 1a illustrates the proposed strategy of FGA formation through the use of a dual-cure adhesive. In this scheme, the thermal/radiation dual-curable adhesive is applied to the adherends and then thermally cured to fix the joint geometry, all in the conventional manner. Further modulation of the mechanical properties along the adhesive joint (Young's modulus in particular) is achieved by designing radiation shielding and optimization of radiation exposure conditions in order to generate gradients in radiation dose along the joint, resulting in local variations in the level of additional radiation-induced crosslinking that occurs.

Research into the formulation of dual-cure adhesives with crosslink densities and Young's moduli that may be significantly altered as a function of radiation dose is a key step in the implementation of the aforementioned scheme. In polymers, high-energy irradiation typically results in a competition between crosslinking and chain scission.²⁵ While epoxy resins are widely used adhesives that display good radiation resistance, ²⁶ degradation nevertheless predominates over crosslinking when conventional epoxy resins are irradiated. 27-29 A strategy that may favor radiation-induced crosslinking as the primary outcome is the introduction of radiation-curable functionalities (such as C=C bonds).^{30,31} In this work, nadic methyl anhydride (NMA), which contains hindered internal C=C bonds, has been combined with the diglycidyl ether of bisphenol A (DGEBA) to provide a basic epoxy formulation from which to work (Figure 1b). To boost the radiation sensitivity of this anhydride-cured epoxy still further, a liquid rubber (carboxy-terminated butadiene acrylonitrile liquid rubber, CTBN, which contains lesshindered/more-reactive C=C bonds) is used as an additive (Figure 1b). In particular, formulations containing varying concentrations of additives have been studied for their ability to undergo radiation-induced crosslinking and modulation of properties (especially Young's modulus) and to yield gradients in such properties. Additionally, γ irradiation-induced changes

Table 1. Formulations of Baseline and CTBN-Modified DGEBA-NMA Epoxy Resins

Epoxy name	DGEBA + NMA matrix (g)	CTBN (g)	CTBN content (wt %)	$n_{C=C} (mmol/cm^3)$	C=O to epoxy ratio
CTBN0	100	0	0.0	3.4	1.95:1
CTBN15	100	15	13.0	5.3	1.95:1
CTBN25	100	25	20.0	6.3	1.96:1
CTBN50	100	50	33.3	8.3	1.98:1
CTBN75	100	75	42.9	9.8	2.01:1

in crosslink density are correlated with glass transition temperature by applying a theory proposed by Shibayama, providing a deeper understanding of the behavior of these materials.

CHARACTERIZATION

Attenuated Total Reflection Fourier-Transform Infrared Spectroscopy. Attenuated total reflection Fouriertransform infrared spectroscopy (ATR-FTIR) of epoxy resins was carried out using a Bruker Tensor 27 instrument in ATR mode with a ZnSe crystal. Background scans were performed before each test. The spectra were measured by accumulating 32 scans at a resolution of 2 cm⁻¹. The wavenumber range was from 750 to 4000 cm⁻¹. The spectra were treated using the OriginPro 9.1 software package. All spectra were normalized to the absorption peak assigned to skeletal vibrations (1507 \pm 2 cm⁻¹) within the aromatic rings present in these materials. The baseline of each spectrum was manually created by anchoring points (12 in total) to regions of the spectra where no absorption bands were observed. The baseline was then subtracted from the original spectrum to generate a baselinecorrected spectrum.

¹³C Solid-State Nuclear Magnetic Resonance Spectroscopy. ¹³C solid-state nuclear magnetic resonance (ss-NMR) spectroscopy was performed using a Bruker AVANCE III HD spectrometer (600 MHz) at 303 K. Specimens were cut into small pieces (approximately $0.5 \times 0.5 \times 0.2 \text{ mm}$) using a box cutter and loaded into a 4 mm zirconium oxide rotor. The rotor was then sealed with a Kel-F cap. The sealed rotor was spun at a rate of 10 kHz after which 64 scans were collected. Chemical shifts were externally referenced to tetramethylsilane.

¹H Nuclear Magnetic Resonance Spectroscopy. ¹H NMR spectra were collected on a JEOL-ESC 400 (400 MHz) spectrometer at 298 K over the course of 256 scans in total. CDCl₃ was selected as the NMR solvent, with residual CHCl₃ present in the solvent acting as the internal standard.

Thermogravimetric Analysis. Thermogravimetric analysis (TGA) was performed with a TA Instruments Discovery TGA. Samples were placed in a platinum pan, equilibrated at 40 °C, and then heated at a rate of 10 °C/min to a maximum temperature of 600 °C in air with a constant purge rate of 25 mL/min. The degradation temperature ($T_{\rm deg}$) was defined as the 5% weight loss temperature in the weight % vs temperature curve

Differential Scanning Calorimetry. Differential scanning calorimetry (DSC) was performed using TA Instruments Discovery DSC. Samples were placed in standard aluminum pans and heated to 120 °C at 5 °C/min, then cooled to -30 °C at 5 °C/min, and finally reheated to 220 °C at 5 °C/min, all in a nitrogen atmosphere with a constant flow rate of 40 mL/min. The $T_{\rm g}$ was obtained from the second heating cycle and was taken from the peak in the first derivative of the heat flow vs temperature curve.

Dynamic Mechanical Analysis. Dynamic mechanical analysis (DMA) was tested via Netzsch GABO EPLEXOR 500 N DMA equipped with a tensile setup. Samples were cut to dimensions of $25 \times 6 \times 1.5$ mm³. The measurements were done in strain-controlled tension mode (0.5% static strain and 0.15% dynamic strain) from -50 to 250 °C at a frequency of 1 Hz. Storage modulus (E'), loss modulus (E''), and loss tangent (tan $\delta = E''/E'$) data were obtained at a heating rate of 3 °C/ min. The T_{α} was defined as the temperature corresponding to the peak in the E'' vs temperature curve. $T_{tan \delta}$ was defined as the temperature corresponding to the peak in the tan δ vs temperature curve. $T_{dE'}$ was defined as the temperature corresponding to the peak in the first derivative of the E' vs temperature curve for CTBN-filled epoxy resins. In some cases, multiple peaks/peak shoulders were observed. In such cases, peak fitting of the first derivative of E' vs temperature curves was performed using the peak analyzer function of OriginPro 9.1 software package to obtain $T_{dE'}$ values for each thermal transition.³² The details of peak fitting and the determination of $T_{dE'}$ of the rubbery $(T_{dE'\text{-rubbery}})$ and rigid $(T_{dE'\text{-rigid}})$ phases are given in the Supporting Information.

The storage modulus in the rubbery plateau region is proportional to crosslink density of the networks. Based on the kinetic theory of rubber elasticity, the crosslink density (n_c) of epoxy networks was estimated from rubbery plateau storage modulus using the following equation 33,34

$$n_{\rm c} = \frac{E'}{3RT}$$

where E' is the storage modulus in the rubbery plateau region (taken here as 50 K above $T_{\tan\delta}$), R is the gas constant, and T is the absolute temperature in K.

Tensile Test. Tensile tests were performed using an Instron 5966 universal testing machine (10 kN load cell) with a crosshead speed of 5 mm/min at 25 °C in accordance with ASTM D638. Tensile specimens were prepared in accordance with the ASTM D638 type-I test specimen specifications. The tensile strain was measured via digital image correlation (DIC). The tensile test bars were spray painted with white and then black spray paint to generate speckle patterns and then conditioned at 23 °C and 50% RH for 40 h before testing. A Canon EOS 80D APS-C DSLR camera equipped with a macrolens (Canon EF-S 60mm f/2.8 Macro USM) was used to take images during the tensile test. The testing results were analyzed via the Ncorr DIC MATLAB program. The tensile toughness is calculated from the area under the stress-strain curve. At least five specimens were tested for every unique combination of epoxy formulation and γ -ray dose.

Shore D Indentation Test. A Fowler type D Shore durometer gauge was used to measure the hardness of specimens. Specimens were characterized according to ASTM D2240.

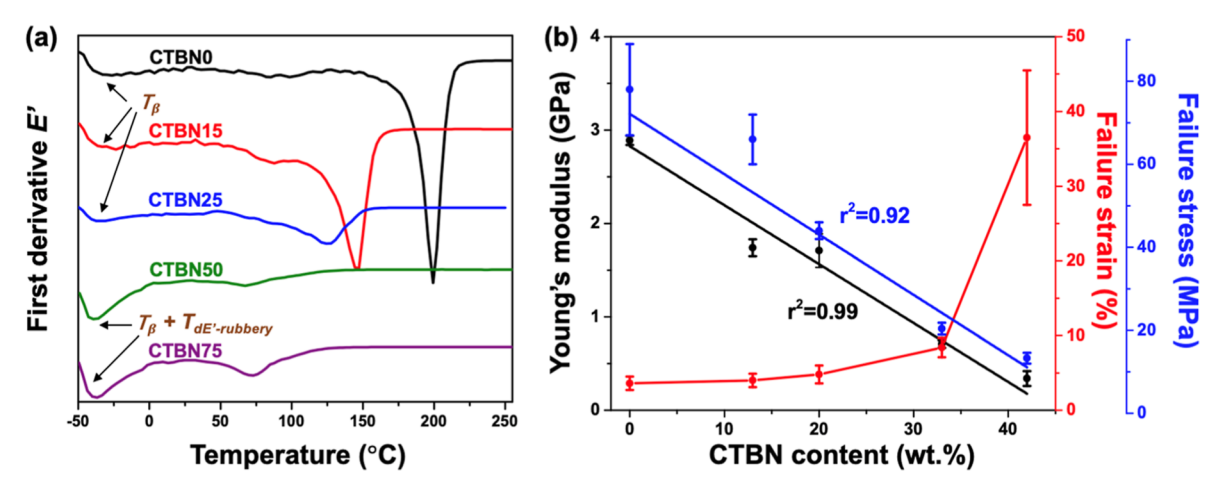


Figure 2. Impact of CTBN addition on thermal and mechanical properties of DGEBA-NMA (CTBN0) epoxy resin. (a) First derivative E' vs temperature of each epoxy resin from DMA; (b) Young's modulus, failure strain and failure stress as a function of CTBN content in the networks from tensile testing; straight lines represent error-weighted linear fits.

RESULTS

CTBN-Filled Epoxy Resins. CTBN is a liquid rubber with high flexibility that increases the toughness of epoxy resins. In addition, the large number of unsaturated groups in CTBN generated from the 1,2- and 1,4-addition of butadiene during polymerization has the potential to be involved in radiation-induced crosslinking reactions. With this in mind, the baseline DGEBA-NMA epoxy formulation is combined with different amounts of CTBN (with the DGEBA-to-NMA molar ratio fixed at 1:1.95 for all formulations, and the epoxy group to carbonyl ratio maintained at \sim 1:2 for each formulation; additional information on the starting materials is provided in the Supporting Information) and then thermally cured. The details of these formulations are summarized in Table 1, and their preparation is described in the Supporting Information.

The addition of CTBN to a rigid, high- $T_{\rm g}$ thermosetting material may cause a reduction in its thermal and mechanical properties. Detailed thermal properties values and crosslink densities of each formulation are summarized in Table S1. Inclusion of CTBN is shown to decrease the thermal stability ($T_{\rm deg}$), crosslink density ($n_{\rm c}$) and glass transition temperature of the baseline DGEBA-NMA formulation (Figure 2a, Table S1). The addition of liquid rubber slows crosslinking by diluting the epoxy and anhydride groups involved in thermal curing, and reduces the crosslink density of the cured epoxy resin as well. ^{38,39} The lower reactivity of the carboxylic acid groups in CTBN as compared with the anhydride groups in NMA may cause further reductions in $T_{\rm g}$ beyond those expected thanks to the incorporation of rubber segments that increase network flexibility and chain mobility.

While all of the systems studied here were homogeneous prior to thermal curing, 40 the addition of large amounts of liquid rubber to the formulation may cause phase separation during epoxy network formation. 41,42 In this work, low concentrations of CTBN were found to be miscible with the epoxy matrix based on DMA results, as shown by the fact that a single glass transition temperature beyond 0 °C (first derivative E' vs temperature curve from DMA) was observed in the CTBN0, CTBN15 and CTBN25 formulations (Figures 2a and S1a-c). In these materials, the weak peak observed below 0 °C is assigned to the β transition (T_{β}) associated with phenyl ring rotation in these networks. With the continued addition of CTBN to the system, the lack of a clear glassy

plateau in the E' vs temperature curves is observed, combined with the broadening of the main relaxation in the E'' vs temperature curves derived from DMA testing of CTBN50 and CTBN75 specimens (Figures 2a and S1d,e). This observation can be explained by the fact that the distribution of chain mobilities in the epoxy matrix becomes broader with the inclusion of liquid rubber. 41,42 In particular, the formation of strong peak below 0 °C that overlaps with the β transition peak in the first derivative E' vs temperature curves of the CTBN50 and CTBN75 epoxy resins may be attributed to the glass transition temperature of a rubber-rich phase $(T_{dE'-rubberv})$, implying that some level of phase separation has occurred thanks to the large amount of CTBN added to these formulations (Figures 2a and S1d). These results are consistent with literature reports that ~15 wt % of a rubber toughening agent provides the best balance of properties in epoxy resins, with further increases in rubber concentration favoring phase separation. 40-42 Nonetheless, while microscale phase separation occurs when higher amounts of liquid rubber are added, consistent with prior reports on the topic, the appearance and uniformity of these systems is maintained and their properties render them acceptable for use. 40

Detailed tensile properties of the various thermally cured epoxy resin formulations studied are given in Table S2. The baseline resin (CTBN0) is rigid and relatively brittle in nature, with a high Young's modulus, low failure strain, and tensile toughness. A systematic reduction in Young's modulus combined with parallel increases in failure strain upon CTBN addition confirms the effect of liquid rubber addition on the mechanical properties of these epoxy networks (Figure 2b). Liquid rubber dissolved in the epoxy matrix functions as a flexibilizer, enhancing toughness (Table S2) while reducing stiffness by decreasing both the crosslink density and interactions between neighboring chains in the network.^{36,44} The reduction in failure stress (Table S2) observed in epoxy resins upon CTBN addition is likewise consistent with the aforementioned reductions in stiffness and interchain interaction strength associated with CTBN as well as related decreases in crosslink density.

Irradiation Following Thermal Curing. Detailed irradiation procedures are given in the Supporting Information. The impact of γ -irradiation on the thermal properties and crosslink density of the epoxies has been evaluated via DMA, TGA, and

ACS Applied Polymer Materials

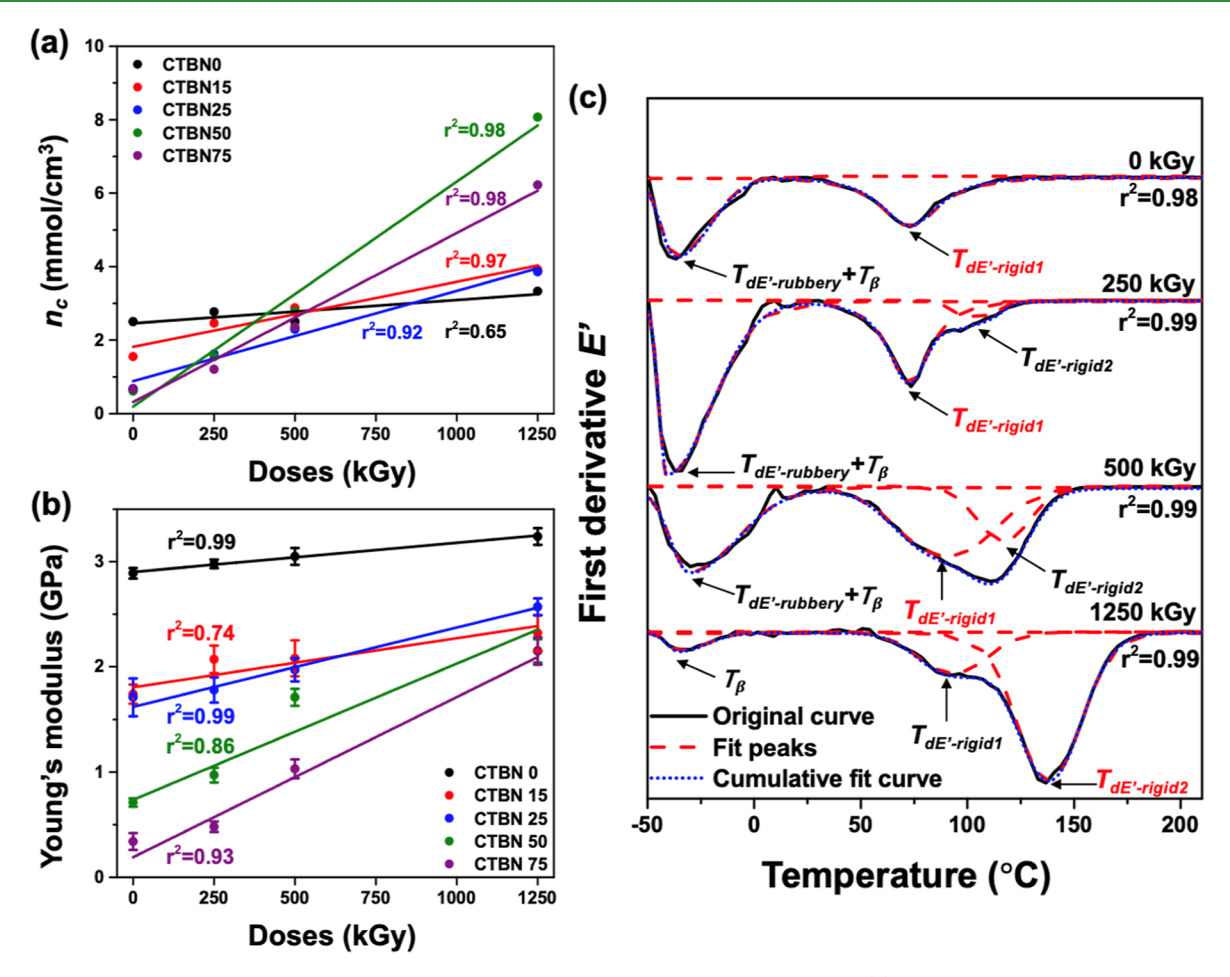


Figure 3. Thermal and mechanical properties of each epoxy resin before and after γ irradiation. (a) n_c vs radiation dose for each epoxy resin formulation studied; (b) Young's modulus vs radiation dose of each epoxy resin formulation studied; and (c) first derivative E' vs temperature for the CTBN75 epoxy resin formulation; the representative $T_{dE'-\text{rigid}}$ value is assigned to whichever transition ($T_{dE'-\text{rigid}}$) is stronger and is identified in red. Lines in (a,b) represent error-weighted linear fits.

DSC (Figures S1–S3), with detailed thermal properties as a function of epoxy resin formulation and dose summarized in Tables S3 and S4. Values of n_c as a function of dose are plotted in Figure 3a. The consistent observation of linear increases in n_c with dose in all CTBN-containing epoxies confirms that the crosslink density in these materials can be effectively modulated by γ irradiation. Additionally, a new peak/shoulder $(T_{dE'\text{-rigid }2})$ is observed in the first derivative E' vs temperature curve, with the strength of the thermomechanical transition increasing with radiation dose (Figures 3c and S1c–e). In the context of this analysis, the strongest high-temperature thermomechanical transition $(T_{dE'\text{-rigid }2})$ at the highest dose) is assigned to the epoxy-rich domain of the multiphase network and is marked with red text in Figure 3c.

Thermal properties of the epoxy-rich domain $(T_{\rm dE'-rigid}, T_{\omega})$ $T_{\rm tan \ \delta}$ and $T_{\rm g1}$) as a function of radiation dose are plotted in Figure S4. Consistent with the changes in $n_{\rm c}$ parallel increases in thermal properties with radiation dose have been observed in CTBN containing epoxy resins. At the highest radiation dose (1250 kGy), the greatest simultaneous increases in $n_{\rm c}$ and all thermal properties $(T_{\rm dE'-rigid}, T_{\rm g1}, T_{\omega})$ and $T_{\rm tan \ \delta}$ are observed in CTBN50 $(n_{\rm c})$ increases by ~1223%, $T_{\rm dE'-rigid}$ increases by ~91 °C, $T_{\rm g1}$ increases by ~42 °C, T_{ω} increases by ~71 °C, and $T_{\rm tan \ \delta}$ increases by ~65 °C), confirming that CTBN addition can significantly boost radiation sensitivity.

For comparison, in the case of the CTBN-free (CTBN0) epoxy control, n_c increases by ~32%, $T_{dE'-rigid}$ increases by ~2 °C, $T_{\rm g1}$ increases by ~7 °C, T_{α} increases by ~1 °C, and $T_{\rm tan~\delta}$ increases by ~3 °C at a dose of 1250 kGy. The fact that the greatest relative increases in crosslink density and thermal properties are not observed in the CTBN75 epoxy resin, in spite of its higher CTBN content, indicates that further addition of liquid rubber additives does not result in still greater radiation sensitivity, likely due to exacerbation of phase separation when such a large amount of CTBN is added. These conclusions are further supported by considering the values of $\Delta n_{\rm c}/n_{\rm C=C}$ vs radiation dose for the formulations studied here (Table S3). These unitless values, which represent the irradiation-induced increase in crosslink density normalized to the total C=C bond content, provide a more objective means of comparing the efficiency of radiation crosslinking between different formulations, with larger values indicating greater radiation sensitivity. As expected, the CTBN0 system shows the lowest values of any system studied, consistent with the low sensitivity expected in the case of the highly hindered C=C bonds present in NMA. The addition of CTBN initially increases the efficiency of radiation crosslinking, with CTBN15 and CTBN25 showing similar levels of sensitivity at all doses. Upon further increases in CTBN content, the CTBN50 formulation shows an even higher level of radiation sensitivity at the highest radiation dose in particular, while CTBN75

ACS Applied Polymer Materials

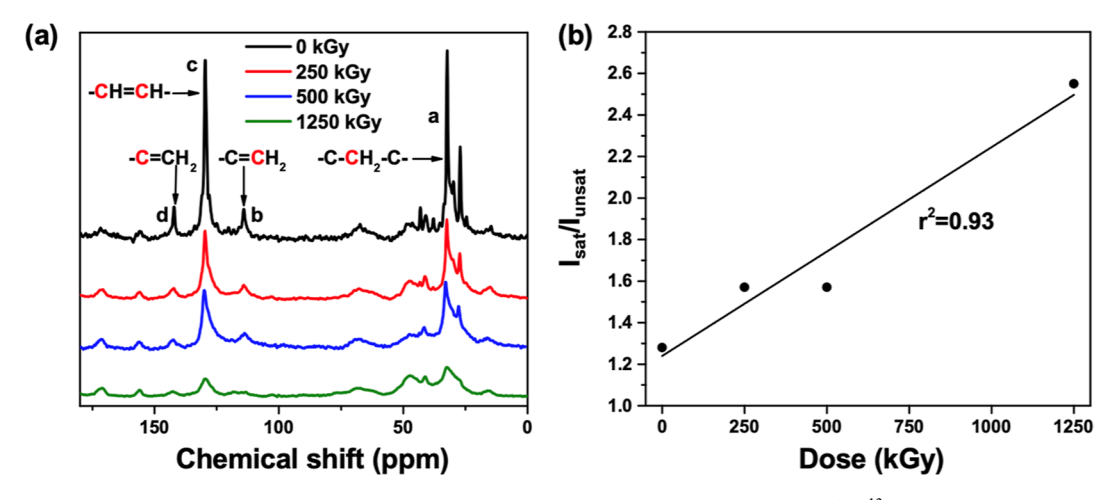


Figure 4. Changes in the structure of a CTBN-containing epoxy resin as a function of radiation dose. (a) 13 C ss-NMR spectra of CTBN50 epoxy resin vs dose and (b) I_{sat}/I_{unsat} of CTBN50 epoxy resin vs dose; line represents a linear fit.

shows reduced radiation sensitivity at all doses vs CTBN50. These results confirm that the addition of the more reactive C=C bonds in CTBN favors radiation crosslinking but that the well-known phenomenon of phase separation when high levels of CTBN are added eventually limits this effect.

In addition to the $T_{\rm dE'-rigid}$ values, $T_{\rm dE'-rubbery}$ is increased with radiation dose as well (250 and 500 kGy, Table S3), to the point where, at 1250 kGy in both the CTBN50 and CTBN75 epoxy resins (Figures 3c and S1d), it has increased so much that only the β transition originally observed in the CTBN-free networks appears to remain. The increase of $T_{\rm dE'-rubbery}$ is consistent with the radiation-induced crosslinking of the rubbery phase, resulting in the formation of highly crosslinked material with a similar glass transition to the neighboring epoxy-rich phase following irradiation at 1250 kGy.

The tensile test results of the thermally cured epoxy formulations studied here before and after γ irradiation are summarized in Table S5. Plots of Young's modulus, failure strain, and failure stress as a function of radiation dose are shown in Figures 3b and S5. In contrast to the neat epoxy, prominent irradiation-induced variations in modulus have been observed in epoxy resins containing CTBN. The good linear fits of the plots indicate that the Young's modulus of CTBNfilled DGEBA-NMA epoxy resins can be effectively modulated by γ -ray dose (Figure 3b). The relative Young's modulus increment (ΔYoung's modulus) achieved following irradiation at 1250 kGy increases linearly with the CTBN content in the formulation (Figure S6), with the greatest increase in modulus (633%) observed in the CTBN75 epoxy resin (vs only 14% for the CTBN-free epoxy resin). CTBN addition has the effect of flexibilizing the epoxy matrix, and large concentrations favor phase separation and the formation of rubbery domains within the network. Radiation-induced crosslinking of the rubber reverses this flexibilizing effect and leads to greater moduli following the irradiation of thermally cured specimens. This explanation is confirmed through the observation of reductions in failure strain with dose in CTBN containing epoxy resins (Figure S5a) as a result of radiation-induced crosslinking. Additionally, increases in failure stress combined with excellent linear fits vs radiation dose confirm once more that crosslinking is the major outcome when CTBN-containing epoxy resins are irradiated following thermal curing (Figure S5b).

Having observed that crosslinking is favored over degradation in these materials, ATR-FTIR was carried out to study the chemical changes in the studied epoxies as a result of irradiation (Figure S7). The changes in the C-H bond absorption bands are useful for assessing both crosslinking and degradation in thermosetting resins. In particular, increases in the strength of the band associated with the C-H asymmetric stretching vibration could be explained by the generation of new C-H bonds in the structure, consistent with crosslinking reactions during γ irradiation. ^{27,37,45} In this work, the combination of a systematic decrease in the intensity of the C=C-H absorption band (965 cm⁻¹, C-H bending vibration in the olefin unit) and an increase in the intensity of the -C-H absorption bands (2917 and 2850 cm⁻¹, C-H stretching vibration in -CH₂- units; 1456 cm⁻¹, bending vibration of C-H) with increasing radiation dose supports the conclusion that crosslinking involving C=C bonds is the major outcome of the irradiation of these CTBN-filled epoxy resins (Figure S7b-e). In comparison, no significant changes can be detected in the CTBN0 formulation before and after irradiation, implying good stability but weak sensitivity of the baseline resin to γ -ray induced crosslinking (Figure S7a). The peak shifts associated with the -C-H absorption bands of the CTBN50 and CTBN75 epoxy resins (from 2913 and 2844 cm⁻¹ at 0 kGy to 2917 and 2850 cm⁻¹ at 1250 kGy) are posited to result from the formation of new alkyl species induced by irradiation. In addition, the significant strengthening of the C-OH absorption band (3510 cm⁻¹, symmetric stretching of O-H in -OH groups) with radiation dose in the CTBN50 and CTBN75 epoxy resin formulations may be explained by the irradiation-induced consumption of residual epoxy groups still present in these materials due to the retarding effects of CTBN on thermal curing (Figure S7d,e).⁴⁶

Although ATR-FTIR is a versatile analytical method that requires minimal sample preparation, it is limited in terms of quantitative analysis of structural changes in materials as the surface roughness of solid samples can affect contact with the ATR crystal and the penetration depth of the evanescent IR wave into the bulk is extremely limited. ATR a result, quantitative comparisons of peak intensities from sample to sample can be challenging, and ATR-FTIR analysis may not provide a representative indication of irradiation-induced changes in structure. This is especially true when composition variations occur over length scales larger than the penetration

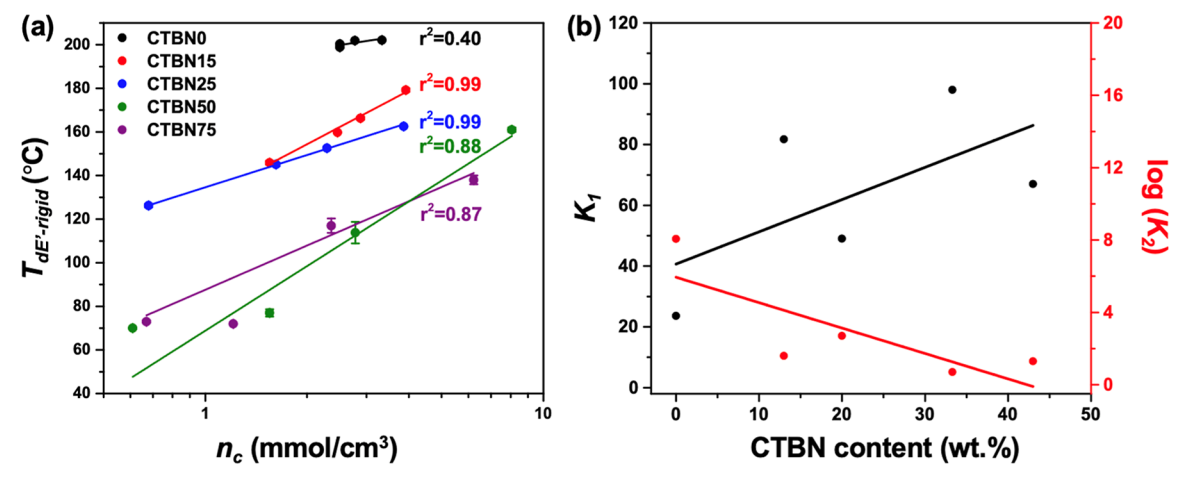


Figure 5. Applying the Shibayama model to radiation postcured epoxy resins. (a) $T_{dE'-rigid}$ vs n_c of each epoxy resin; lines represent linear fits revealing a clear quantitative relationship; (b) K_1 and log (K_2) as a function of CTBN content in the networks; lines represent linear fits intended to guide the eye and reveal general trends.

depth, as can be the case in phase-separated materials. To develop a deeper understanding of the structural changes that occur in CTBN-containing epoxy resins upon irradiation, ¹³C ss-NMR analysis has been carried out to study the structural changes in CTBN50 epoxy networks as a function of dose. The (solution) ¹³C NMR reference spectra of the individual starting materials (DGEBA, NMA and CTBN) and peak assignments for ¹³C ss-NMR measurements of CTBN50 for a structure representative of the network are given in Figure S8. The ¹³C ss-NMR spectra of CTBN50 at each dose are shown in Figure 4a. Even though the ¹³C NMR peaks assigned to the benzene rings in DGEBA (peaks g, f, and e in Figure S8a) partially overlap with the peaks assigned to the C=C bonds of CTBN (peaks a, b, g, and f in Figure S8c) and NMA (peak b in Figure S8b), the changes in shape and intensity of the peaks b (114 ppm), c (129 ppm), and d (142 ppm) in Figure 4a are attributed primarily to the consumption of C=C bonds in the polybutadiene units of the CTBN, given the much higher stability of benzene rings upon irradiation.²² With radiation exposure, the observation of broadening of the initially sharp peaks associated with saturated carbons (peak a, 32 ppm) can be explained by the loss of mobility of the liquid rubber upon radiation crosslinking (Figure 4a). To quantify new bond formation and relate it to consumption of unsaturated species in the network, integration ratios between peaks a and c ($I_{\rm sat}/$ I_{unsat}) are calculated and plotted as a function of radiation dose (Figure 4b). The observation of a linear increase in the value of $I_{\rm sat}/I_{\rm unsat}$ further supports the conclusion that the structure of the crosslinked polymer network is effectively and consistently modulated by γ irradiation through the reaction of C=C

Applying Shibayama Theory. In 1961, Shibayama proposed a theory that has been used to describe the behavior of thermosetting resins by relating glass transition temperature with crosslink density based on the reduction in free volume resulting from crosslinking and suggested the following equation that he then applied successfully to many thermosetting resins⁴⁹

$$T_{g}(^{\circ}C) = K_{1}\log(K_{2} \cdot n_{c}) = K_{1}\log(K_{2}) + K_{1}\log(n_{c})$$

Here, K_1 and log (K_2) are constants. The constant K_1 reflects the degree of restraint on local chain mobility imposed by the addition of a new crosslink (higher K_1 values imply more

significant local reductions in chain mobility imposed by the addition of new crosslinks). The constant $\log{(K_2)}$ characterizes the interactions and rigidity of the chains between the crosslinks [higher $\log{(K_2)}$ values indicate more significant interaction between chains/higher chain rigidity].

The Shibayama model has been successfully applied to evaluate the rigidity of new formed crosslinks in networks upon thermal curing, reflecting the degree of restraint on local chain mobility imposed by the addition of a new crosslink. 16,50 An examination of K_1 and log (K_2) values for the systems described here may therefore provide a deeper understanding of the crosslinking behavior and chain structures of these dualcure epoxy resins when they are subjected to γ irradiation. With this in mind, the Shibayama model is applied to this work by creating linear fits for plots of $T_{\rm dE'-rigid}$ vs $n_{\rm c}$ at each dose level (Figure 5a). Some scatter observed in the data of CTBN50 and CTBN75 networks is due to the phase separation and radiation-induced crosslinking/degradation in both the rubbery and epoxy matrix phases increasing uncertainties as far as the glass transition temperature of these materials is concerned. The values of K_1 and log (K_2) obtained from linear fitting of the data for each epoxy resin system are listed in Table S6. The low K_1 values coupled with high $\log (K_2)$ values of the CTBN0 epoxy resin imply that radiation crosslinking produces limited reductions in local chain mobility and that the chains between crosslinks in this network are quite rigid. These results are consistent with expectations based on the structure of the molecules making up this network and in agreement with the limited increase in Young's modulus of the CTBN0 epoxy resin following irradiation. K_1 and log (K_2) values are plotted as a function of liquid rubber content (Figure 5b). While the application of the Shibayama model to liquid rubber-filled epoxy is complicated by the fact that some degree of phase separation occurs during curing at higher CTBN contents (Figure 2a), this model is nonetheless robust enough to reveal logical trends in the fitting parameters. In particular, the addition of CTBN increases K_1 but decreases $\log (K_2)$, implying that the crosslinking of C=C bonds in a less-rigid network structure results in more local constraints on chain motion—again, consistent with expectations given the inherently flexible nature of the rubber segments prior to crosslinking. This result explains the progressively larger radiation-induced

increases in Young's modulus as CTBN content is increased in the DGEBA-NMA epoxy resin system and reconfirms the capacity of CTBN to enhance radiation sensitivity in these resin formulations. Likewise, the use of the Shibayama model provides useful insights into the behavior of these materials and the consequences of radiation-induced crosslinking, which in turn help to inform the observed changes in Young's modulus as well.

Generation of FGMs. The proposed technique for FGA production may be applied to create FGMs as well. To verify the potential of these dual-cure epoxies to enable the generation of FGAs, an FGM has been prepared via the general methodology proposed in this work (Figure 1), as illustrated more specifically in Figure 6a. A machined steel

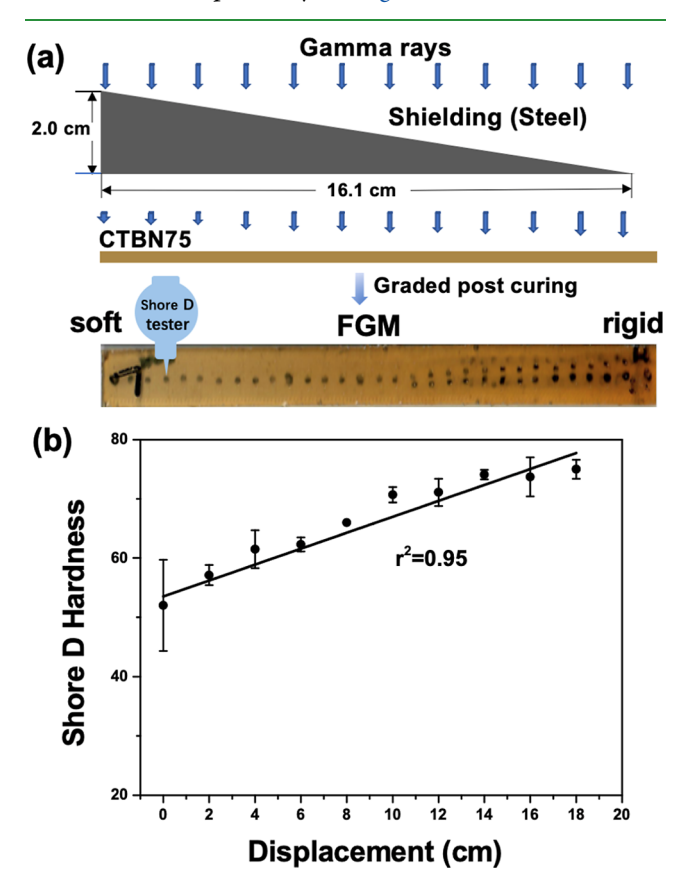


Figure 6. Generation of FGMs via the proposed method: (a) schematic illustration of the generation of FGMs via graded post cure and an image of an FGM specimen created in this way; (b) plot of Shore D hardness results for an FGM specimen as a function of position [from the shielded to the unshielded end; (a)] of the tester; line represents error-weighted linear fit.

(half value layer vs 60 Co γ -rays = 2.1 cm) with varied thickness is selected as radiation shield to be placed between a radiation source and a thermally cured CTBN75 epoxy resin specimen and then postcured at an unshielded (maximum) dose of 500 kGy. Following irradiation with a graded dose profile, the observation of a continuous change in the color of the specimen from light yellow to brown is a direct indication of the generation of a gradient in chemical structure (Figure 6a). Figure 6b shows the Shore D hardness values of graded post cured specimen as a function of position along the specimen from the highly shielded end to the unshielded end. The linear increase in hardness confirms the generation of an FGM and

the ability to program the stiffness of the material via the proposed method.

CONCLUSIONS

Herein, we proposed a general approach to the preparation of FGAs via the formulation of thermal/ionizing radiation dualcured resins. To realize this approach in practice, epoxy resins designed to exhibit crosslink densities and mechanical properties that may be precisely tuned via irradiation following thermal curing have been developed, and their structureproperty relationships have been clarified. An unsaturated liquid anhydride (NMA) was selected as the hardener and combined with a conventional epoxy monomer (DGEBA) to generate a baseline formulation for this effort. The baseline DGEBA-NMA epoxy displayed some inherent capacity for modulation of Young's modulus by γ irradiation, but larger radiation-induced variations in Young's modulus were desired for FGA formation. To address this issue, an unsaturated liquid rubber (CTBN) was selected as a reactive additive and added to the DGEBA-NMA formulation prior to network formation. It was observed that CTBN addition boosted the radiation sensitivity of the epoxy resin and that the crosslink density and thermal and mechanical properties were all effectively and significantly modulated by γ irradiation in those systems containing CTBN. As a direct comparison, n_c increases by \sim 1223%, $T_{\rm dE'-rigid}$ increases by \sim 91 °C, and Young's modulus increases by 200% for the CTBN50 epoxy resin at 1250 kGy, while n_c increases by ~32%, $T_{\rm dE'-rigid}$ increases by ~3 °C, and Young's modulus increases by 14% for the baseline CTBN0 epoxy resin. 13C ss-NMR was carried out to quantify the consumption of unsaturation and the formation of radiationinduced crosslinks. In addition, Shibayama theory was successfully applied to these thermal/radiation dual-cured networks. The application of this model revealed that CTBN lowered chain rigidity [reducing the log (K_2) value vs DGEBA-NMA], while irradiation-induced crosslinking of unsaturations in the CTBN imposed strong local restrictions on chain motion (increasing the K_1 value vs DGEBA-NMA), providing useful insights into the behavior of these systems and the origins of the observed variations in Young's modulus. Finally, the irradiation of a CTBN-filled epoxy through an appropriate geometry of (graded) radiation shielding enabled the generation of a specimen with a clear gradient in both appearance and hardness, confirming the potential of these materials and the proposed method of locally modulating their properties as a means of generating FGAs. Such work is already in progress, with a subsequent report in preparation focused on the mechanical aspects of FGA design and testing using these materials as a basis.

ASSOCIATED CONTENT

Supporting Information

The Supporting Information is available free of charge at https://pubs.acs.org/doi/10.1021/acsapm.3c00465.

Chemical information; preparation of epoxy resin; radiation post curing and characterization results of DMA, DSC, TGA, and tensile testing, and FTIR and NMR analysis (PDF)

AUTHOR INFORMATION

Corresponding Author

Daniel F. Schmidt — Department of Plastics Engineering, University of Massachusetts Lowell, Lowell, Massachusetts 01854, United States; Department of Materials Research & Technology, Luxembourg Institute of Science & Technology, Hautcharage L-4940, Luxembourg; ⊚ orcid.org/0000-0003-2511-1906; Email: daniel.schmidt@list.lu

Authors

- Weiqing Xia Department of Plastics Engineering, University of Massachusetts Lowell, Lowell, Massachusetts 01854, United States
- Samuel B. Hurvitz Department of Mechanical Engineering, University of Massachusetts Lowell, Lowell, Massachusetts 01854, United States
- Joshua Y. Lee Department of Mechanical Engineering, University of Massachusetts Lowell, Lowell, Massachusetts 01854, United States
- Scott E. Stapleton Department of Mechanical Engineering, University of Massachusetts Lowell, Lowell, Massachusetts 01854, United States; orcid.org/0000-0003-4834-9992

Complete contact information is available at: https://pubs.acs.org/10.1021/acsapm.3c00465

Author Contributions

All authors have given approval to the final version of the manuscript.

Funding

This material is based upon work supported by the National Science Foundation under grant no 1663502.

Notes

The authors declare no competing financial interest.

■ ACKNOWLEDGMENTS

The authors gratefully acknowledge the support and assistance of Mary Montesalvo, Ksenofon Konomi, and the UMass Lowell Radiation Laboratory in performing the γ -ray exposures described. They thank Dr. Reiner Dieden, Dr. Chuanyu Yan, and Dr. Adrien Comès of the Luxembourg Institute of Science and Technology for support and assistance with ss-NMR testing and data analysis. They thank Benoit Marcolini of the Luxembourg Institute of Science and Technology for thermal characterization. They thank Yunchuan Qi at the University of Massachusetts Lowell for assistance with solution NMR spectroscopy. They also thank Dr. Sara Najafian, Alessandro Cassano and Jamal Husseini at the University of Massachusetts Lowell for assistance with the preparation and characterization of selected materials. Finally, they would like to thank the Department of Materials Research & Technology at the Luxembourg Institute of Science and Technology for hosting W. Xia and providing him with access to the facilities and support needed to complete this effort.

■ REFERENCES

- (1) Suresh, S. Graded Materials for Resistance to Contact Deformation and Damage. *Science* **2001**, *292*, 2447–2451.
- (2) Sato, M.; Inoue, A.; Shima, H. Bamboo-İnspired Optimal Design for Functionally Graded Hollow Cylinders. *PLoS One* **2017**, *12*, No. e0175029.
- (3) Dao, M.; Gu, P.; Maewal, A.; Asaro, R. J. A Micromechanical Study of Residual Stresses in Functionally Graded Materials. *Acta Mater.* **1997**, *45*, 3265–3276.

- (4) Almasi, D.; Sadeghi, M.; Lau, W. J.; Roozbahani, F.; Iqbal, N. Functionally Graded Polymeric Materials: A Brif Review of Current Fabrication Methods and Introduction of a Novel Fabrication Method. *Mater. Sci. Eng. C* **2016**, *64*, 102–107.
- (5) Naebe, M.; Shirvanimoghaddam, K. Functionally Graded Materials: A Review of Fabrication and Properties. *Appl. Mater. Today* **2016**, *5*, 223–245.
- (6) Lowen, J. M.; Leach, J. K. Functionally Graded Biomaterials for Use as Model Systems and Replacement Tissues. *Adv. Funct. Mater.* **2020**, *30*, 1909089.
- (7) Nuvoli, D.; Alzari, V.; Pojman, J. A.; Sanna, V.; Ruiu, A.; Sanna, D.; Malucelli, G.; Mariani, A. Synthesis and Characterization of Functionally Gradient Materials Obtained by Frontal Polymerization. *ACS Appl. Mater. Interfaces* **2015**, *7*, 3600–3606.
- (8) Haring, A. P.; Khan, A. U.; Liu, G.; Johnson, B. N. 3D Printed Functionally Graded Plasmonic Constructs. *Adv. Opt. Mater.* **2017**, *5*, 1700367.
- (9) Stapleton, S. E.; Weimer, J.; Spengler, J. Design of Functionally Graded Joints Using a Polyurethane-Based Adhesive with Varying Amounts of Acrylate. *Int. J. Adhes. Adhes.* **2017**, *76*, 38–46.
- (10) Stein, N.; Mardani, H.; Becker, W. An Efficient Analysis Model for Functionally Graded Adhesive Single Lap Joints. *Int. J. Adhes. Adhes.* **2016**, *70*, 117–125.
- (11) Raphael, C. Variable-adhesive bonded joints. *Applied Polymer Symposium*, 1966; Vol. 3, pp 99–108.
- (12) Stapleton, S. E.; Waas, A. M.; Arnold, S. M. Functionally Graded Adhesives for Composite Joints. *Int. J. Adhes. Adhes.* **2012**, *35*, 36–49.
- (13) Kumar, S. Analysis of Tubular Adhesive Joints with a Functionally Modulus Graded Bondline Subjected to Axial Loads. *Int. J. Adhes. Adhes.* **2009**, *29*, 785–795.
- (14) Marques, J. B.; Barbosa, A. Q.; da Silva, C. I.; Carbas, R. J. C.; da Silva, L. F. M. An Overview of Manufacturing Functionally Graded Adhesives Challenges and Prospects. *J. Adhes.* **2021**, *97*, 172–206.
- (15) Durodola, J. F. Functionally Graded Adhesive Joints A Review and Prospects. *Int. J. Adhes. Adhes.* **2017**, *76*, 83–89.
- (16) Xia, W.; Najafian, S.; Cassano, A. G.; Stapleton, S. E.; Schmidt, D. F. Functionally Graded Adhesives via High-Energy Irradiation. *ACS Appl. Polym. Mater.* **2021**, *3*, 104–109.
- (17) Ker, D. F. E.; Wang, D.; Behn, A. W.; Wang, E. T. H.; Zhang, X.; Zhou, B. Y.; Mercado-Pagán, Á. E.; Kim, S.; Kleimeyer, J.; Gharaibeh, B.; Shanjani, Y.; Nelson, D.; Safran, M.; Cheung, E.; Campbell, P.; Yang, Y. P. Functionally Graded, Bone- and Tendon-Like Polyurethane for Rotator Cuff Repair. *Adv. Funct. Mater.* **2018**, 28, 1707107.
- (18) dos Santos, G. B.; Alto, R. M.; Filho, H. S.; da Silva, E. M.; Fellows, C. E. Light Transmission on Dental Resin Composites. *Dent. Mater.* **2008**, 24, 571–576.
- (19) Kawasaki, S.; Nakajima, G.; Haraga, K.; Sato, C. Functionally Graded Adhesive Joints Bonded by Honeymoon Adhesion Using Two Types of Second Generation Acrylic Adhesives of Two Components. *J. Adhes.* **2016**, *92*, 517–534.
- (20) Bonaldo, J.; Banea, M. D.; Carbas, R. J. C.; Da Silva, L. F. M.; De Barros, S. Functionally Graded Adhesive Joints by Using Thermally Expandable Particles. *J. Adhes.* **2019**, *95*, *995*–1014.
- (21) Carbas, R. J. C.; da Silva, L. F. M.; Critchlow, G. W. Adhesively Bonded Functionally Graded Joints by Induction Heating. *Int. J. Adhes. Adhes.* **2014**, *48*, 110–118.
- (22) Hu, W. H.; Tenjimbayashi, M.; Wang, S.; Nakamura, Y.; Watanabe, I.; Naito, M. Postprogrammable Network Topology with Broad Gradients of Mechanical Properties for Reliable Polymer Material Engineering. *Chem. Mater.* **2021**, *33*, 6876–6884.
- (23) Carbas, R. J. C.; da Silva, L. F. M.; Marques, E. A. S.; Lopes, A. M. Effect of Post-Cure on the Glass Transition Temperature and Mechanical Properties of Epoxy Adhesives. *J. Adhes. Sci. Technol.* **2013**, 27, 2542–2557.
- (24) Xia, W. Dual curable epoxy resins enabling functionally graded adhesives. Ph.D. Thesis, University of Massachusetts Lowell, 2022.

ı

- (25) Diao, F.; Zhang, Y.; Liu, Y.; Fang, J.; Luan, W. γ-Ray Irradiation Stability and Damage Mechanism of Glycidyl Amine Epoxy Resin. *Nucl. Instrum. Methods Phys. Res. Sect. B Beam Interact. Mater. Atoms* **2016**, 383, 227–233.
- (26) Gilfrich, H.-P.; Wilski, H. The Radiation Resistance of Thermoset Plastics—V. Epoxy Plastics. *Int. J. Radiat. Appl. Instrum. C Radiat. Phys. Chem.* **1992**, 39, 401–405.
- (27) Xing, A.; Bai, Y.; Wen, Y.; Zhao, F.; Meng, Y.; Li, X. Effects of γ Irradiation on the Structure, Physical and Mechanical Properties of a Series of Tetrafunctional Epoxies Modified DGEBA/DDS. *Mater. Today Commun.* **2021**, 27, 102337.
- (28) Zimmermann, J.; Sadeghi, M. Z.; Schroeder, K. U. The Effect of γ -Radiation on the Mechanical Properties of Structural Adhesive. *Int. J. Adhes. Adhes.* **2019**, 93, 102334.
- (29) Zimmermann, J.; Schalm, T.; Sadeghi, M. Z.; Schröder, K. U. Empirical Investigations on the Effects of Ionizing Radiation on Epoxy Structural Adhesives and Resins: An Overview. *Int. J. Adhes. Adhes.* **2022**, *117*, 103014.
- (30) Hoffman, A. S.; Jameson, J. T.; Salmon, W. A.; Smith, D. E.; Trageser, D. A. Electron Radiation Curing of Styrene-Polyester Mixtures. Effect of Backbone Reactivity and Dose Rate. *Ind. Eng. Chem. Prod. Res. Dev.* **1970**, *9*, 158–167.
- (31) Rezaei Abadchi, M.; Jalali-Arani, A. The Use of Gamma Irradiation in Preparation of Polybutadiene Rubber Nanopowder; Its Effect on Particle Size, Morphology and Crosslink Structure of the Powder. Nucl. Instrum. Methods Phys. Res. Sect. B Beam Interact. Mater. Atoms 2014, 320, 1–5.
- (32) Dunkerley, E.; Schmidt, D. F. Understanding the Consequences of Intercalation Using Model Polymer Nanolaminates. *Macromolecules* **2015**, *48*, 7620–7630.
- (33) Andjelkovic, D. D.; Valverde, M.; Henna, P.; Li, F.; Larock, R. C. Novel Thermosets Prepared by Cationic Copolymerization of Various Vegetable Oils—Synthesis and Their Structure—Property Relationships. *Polymer* **2005**, *46*, 9674—9685.
- (34) Hill, L. W. Calculation of Crosslink Density in Short Chain Networks. *Prog. Org. Coat.* **1997**, *31*, 235–243.
- (35) Bagheri, R.; Marouf, B. T.; Pearson, R. A. Rubber-Toughened Epoxies: A Critical Review. *Polym. Rev.* **2009**, *49*, 201–225.
- (36) Hassan, M. M.; Aly, R. Ó.; El-Ghandour, A.; Abdelnaby, H. A. Effect of Gamma Irradiation on Some Properties of Reclaimed Rubber/Nitrile—Butadiene Rubber Blend and Its Swelling in Motor and Brake Oils. *J. Elastomers Plast.* **2013**, *45*, 77—94.
- (37) Taewattana, R.; Jubsilp, C.; Suwanmala, P.; Rimdusit, S. Effect of Gamma Irradiation on Properties of Ultrafine Rubbers as Toughening Filler in Polybenzoxazine. *Radiat. Phys. Chem.* **2018**, 145, 184–192.
- (38) Wise, C. W.; Cook, W. D.; Goodwin, A. A. CTBN Rubber Phase Precipitation in Model Epoxy Resins. *Polymer* **2000**, *41*, 4625–4633.
- (39) Bascom, W. D.; Cottington, R. L.; Jones, R. L.; Peyser, P. The Fracture of Epoxy- and Elastomer-Modified Epoxy Polymers in Bulk and as Adhesives. *J. Appl. Polym. Sci.* 1975, 19, 2545–2562.
- (40) Ratna, D.; Banthia, A. K. Rubber Toughened Epoxy. *Macromol. Res.* **2004**, *12*, 11–21.
- (41) Thomas, R.; Durix, S.; Sinturel, C.; Omonov, T.; Goossens, S.; Groeninckx, G.; Moldenaers, P.; Thomas, S. Cure Kinetics, Morphology and Miscibility of Modified DGEBA-Based Epoxy Resin Effects of a Liquid Rubber Inclusion. *Polymer* **2007**, *48*, 1695–1710.
- (42) Thomas, R.; Abraham, J.; Thomas P, S.; Thomas, S. Influence of Carboxyl-Terminated (Butadiene-Co-Acrylonitrile) Loading on the Mechanical and Thermal Properties of Cured Epoxy Blends. *J. Polym. Sci., Part B: Polym. Phys.* **2004**, 42, 2531–2544.
- (43) Foreman, J. P.; Porter, D.; Behzadi, S.; Jones, F. R. A Model for the Prediction of Structure—Property Relations in Cross-Linked Polymers. *Polymer* **2008**, *49*, 5588—5595.
- (44) Liaw, D.-J.; Liaw, B.-Y.; Yang, C.-M. Synthesis and Characterization of New Soluble Cardo Aromatic Polyamides Bearing

- Diphenylmethylene Linkage and Norbornyl Group. *Macromol. Chem. Phys.* **2001**, 202, 1866–1872.
- (45) Schissel, S. M.; Lapin, S. C.; Jessop, J. L. P. Characterization and Prediction of Monomer-Based Dose Rate Effects in Electron-Beam Polymerization. *Radiat. Phys. Chem.* **2017**, *141*, 41–49.
- (46) Wang, X.; Soucek, M. D. Spectroscopy Analysis of Micro/Nanostructured Epoxy/Rubber Blends. In *Micro- and Nanostructured Epoxy/Rubber Blends*; Thomas, S., Sinturel, C., Thomas, R., Eds.; Wiley-VCH Verlag GmbH & Co. KGaA: Weinheim, Germany, 2014; pp 315–338.
- (47) Gulmine, J. V.; Janissek, P. R.; Heise, H. M.; Akcelrud, L. Polyethylene Characterization by FTIR. *Polym. Test.* **2002**, *21*, 557–563.
- (48) Cornel, J.; Lindenberg, C.; Mazzotti, M. Quantitative Application of in Situ ATR-FTIR and Raman Spectroscopy in Crystallization Processes. *Ind. Eng. Chem. Res.* **2008**, *47*, 4870–4882.
- (49) Shibayama, K. Glass Transition Temperature of Crosslinked Polymer. Kobunshi Kagaku 1961, 18, 183–186.
- (50) Shibayama, K. Temperature Dependence of the Physical Properties of Crosslinked Polymers. *Prog. Org. Coat.* **1975**, *3*, 245–260.